HHS Public Access

Author manuscript

Cell Rep. Author manuscript; available in PMC 2021 October 14.

Published in final edited form as:

Cell Rep. 2021 March 16; 34(11): 108871. doi:10.1016/j.celrep.2021.108871.

Circuit reorganization in the *Drosophila* mushroom body calyx accompanies memory consolidation

Lothar Baltruschat[1,¶], **Luigi Prisco**[1,¶], **Philipp Ranft**[1,¶], **J. Scott Lauritzen**[2], **André Fiala**[3], **Davi D. Bock**[2,4], **Gaia Tavosanis**[1,5,6,*]

[1]Center for Neurodegenerative Diseases (DZNE), 53175 Bonn, Germany

[2]Janelia Research Campus, Howard Hughes Medical Institute, Ashburn, VA 20147, United States

[3]Molecular Neurobiology of Behaviour, University of Göttingen, 37077 Germany

[4]Department of Neurological Sciences, University of Vermont, Burlington, VT 05405, USA

[5]LIMES Institute, University of Bonn, 53115 Germany

[6]Lead Contact

Summary

The formation and consolidation of memories are complex phenomena involving synaptic plasticity, microcircuit reorganization and the formation of multiple representations within distinct circuits. To gain insight on the structural aspects of memory consolidation, we focus on the calyx of the *Drosophila* mushroom body. In this essential centre essential for olfactory learning, second and third order neurons connect through large synaptic microglomeruli that we dissect at the electron microscopy level. Focussing on microglomeruli that respond to a specific odor, we reveal that appetitive long-term memory results in increased numbers precisely of those functional microglomeruli responding to the conditioned odor. Hindering memory consolidation by non-coincident presentation of odor and reward, by blocking protein synthesis or including memory mutants suppress these structural changes, revealing their tight correlation with the process of memory consolidation. Thus, olfactory long-term memory is associated with input-specific structural modifications in a high-order centre of the fly brain.

Keywords

Drosophila ; structural plasticity; functional plasticity; memory consolidation; mushroom body; microglomerulus

[*]To whom correspondence should be addressed. gaia.tavosanis@dzne.de.

[¶]Equal contribution

Author Contributions

L.B. and G.T. conceived the project and designed the experiments. L.B., P.R. and L.P. constructed fly strains, performed behavioural experiments, produced and analysed the anatomical data. J.S.L. and D.D.B. established the set of EM data and P.R. performed the tracings presented here. Scripts and routines for the analysis were established by L.B. and L.P. Functional imaging experiments were designed and performed by L.B and L.P. with support by A.F. The manuscript was written by G.T, L.B., P.R and L.P.

Declaration of Interests

The authors declare no competing interests.

Introduction

The capacity of utilizing past experience to guide future action is a fundamental and conserved function of the nervous system. Associative memory formation initiated by the coincident detection of a conditioned stimulus (CS, e.g. odor) and an unconditioned stimulus (US, e.g. sugar reward) leads to a short-lived memory trace (STM) within distinct circuits (Josselyn and Tonegawa, 2020, Boto et al., 2020, Wang et al., 2008, Liu et al., 2012, Burke et al., 2012). Memories can be consolidated into long-term memories (LTM) through processes that depend on *de-novo* protein synthesis (Tully et al., 1994, Bailey et al., 1996), require structural modifications within the involved neuronal circuits and might lead to the recruitment of additional ones (Dubnau and Chiang, 2013, Cervantes-Sandoval et al., 2013, Kitamura and Ogawa, 2017, Caroni et al., 2012, Holtmaat and Caroni, 2016, Kleim et al., 2002, Hihara et al., 2006, Bassett et al., 2011, Gu et al., 2015, Maviel et al., 2004). Compared to modulation of existing connections, the reorganization of circuits affords the unique possibility of sampling for potential new partners (Chklovskii et al., 2004, Gogolla et al., 2007, Bennett et al., 2018). Nonetheless, only few examples of rewiring associated with learning have been established thus far (Boele et al., 2013, Hihara et al., 2006, Chen et al., 2015, Poort et al., 2015, Grewe et al., 2017).

The formation and retrieval of olfactory associative memories in *Drosophila* requires the mushroom body (de Belle and Heisenberg, 1994). Within the main MB input compartment, the calyx (MBC), second order projection neurons (PNs) deliver olfactory information through cholinergic synapses to the intrinsic MB neurons, the Kenyon cells (KCs, Figure 1A). In the MBC, large olfactory PN boutons are enwrapped by the claw-like dendrite termini of ~11 KCs on average (Butcher et al., 2012, Caron et al., 2013), thereby forming characteristic synaptic complexes, the microglomeruli (Yasuyama et al., 2002), which display functional and structural plasticity in adaptation and upon silencing (Kremer et al., 2010, Pech et al., 2015, Leiss et al., 2009). To start addressing systematically the mechanisms that support memory consolidation, we sought to investigate the properties of identifiable synaptic MGs in the MB of the adult brain of *Drosophila* after the establishment of LTM.

Combining behavioural experiments with high-resolution microscopy and functional imaging, we demonstrate that the consolidation of appetitive olfactory memories closely correlates with an increase in the number of MGs formed by the PNs that deliver the conditioned stimulus and their postsynaptic KC partners. These structural changes result in additional functional synaptic connections. Thus, the circuit in the calyx of the fly MB reorganizes accompanying the consolidation of associative memories.

Results

Identifiable synaptic microglomeruli in the calyx respond to cVA

To reveal potential changes in synapse organization linked to memory consolidation, we first developed a setup allowing to identify the individual synapses of olfactory PNs that deliver a conditioned odor to the MB. The pheromone and odorant 11-cis-Vaccenylacetate (cVA) specifically activates PNs that project their dendrites to the DA1 glomerulus in the

antennal lobe (AL) (Datta et al., 2008, Kurtovic et al., 2007, Schlief and Wilson, 2007). The DA1 glomerulus is mostly excluded from complex processing of sensory information in the AL (Lebreton et al., 2014, Lebreton et al., 2015), suggesting that by genetically marking the DA1 PNs we could identify the individual boutons in the MBC that deliver the olfactory response to cVA. We tested this by recording with volumetric calcium imaging the response to odor stimulation in the MBC of animals expressing a genetically encoded calcium indicator tethered at the KC postsynapses (Pech et al., 2015) in combination with a presynaptic fluorescent tag (*UAS-tdTomato*) expressed in DA1-PNs only (Figure 1C). Regions of interest (ROIs) containing fluorescently labelled DA1-MGs showed a postsynaptic response specifically tuned to cVA stimulation (84% ± 8 of the fluorescently labelled DA1-MGs responded to cVA and not to the solvent alone, 9% ± 7 did not respond to cVA or solvent, 7% ± 5 responded to both. Data expressed as mean ± std, n=7, Figure 1C).

Therefore, by selecting the combination of the cVA odorant and the DA1 subset of PNs we established a system in which we can track a fly's neuronal response towards a specific odor on the level of individual synaptic complexes in the MBC (Figure 1A–C).

To gain insight into the complexity of the MG microcircuit formed by a single DA1-PN bouton we took advantage of the availability of an adult whole brain electron microscopy (EM) volume (Zheng et al., 2018). With this dataset, we reconstructed a complete MG connectome by tracing neurites from every pre- and postsynaptic contact of a DA1-PN bouton until the corresponding neuron's identity was anatomically determinable (Figure 1D, E; Supplementary Table 1). This particular DA1-PN bouton made 33 excitatory cholinergic contacts, all polyadic and identifiable by the presence of a T-bar and a synaptic cleft (Figure 1E, inset), apposed to 277 postsynaptic profiles. Most profiles (248) postsynaptic to the bouton originated from 14 KCs of 5 different subtypes: γmain (8), αβs (3), αβc (1), α'β'ap (1) and α'β'm (1) (Aso et al., 2014). γmain profiles were the most abundant in this particular bouton, although DA1-PN boutons are located within a region of the MBC predominantly occupied by αβs KCs (Lin et al., 2007). Each KC contacted the bouton with a single claw receiving 8 to 25 presynaptic inputs from the PN bouton, in line with previous estimates (Butcher et al., 2012, Leiss et al., 2009). Within the MG, the bouton received presynaptic input from 4 cells: two additional γmain KCs forming divergent triads that included a KC, the PN bouton and the anterior paired lateral neuron (Liu and Davis, 2009); APL itself and one of the two Mushroom Body Calyx 1 neurons (MB-C1) (Supplementary Table 1). Taken together, a single MG represents a highly complex microcircuit, involving many neurons (19 in this example) of different types (here 8).

Structural changes in calycal microglomeruli upon memory consolidation

To investigate whether such a complex structure undergoes plastic changes, we designed a setup to observe and measure the properties of identifiable MGs following olfactory conditioning.

In confocal images, we highlighted cVA responsive MGs in the MBC by expressing the presynaptic active zone (AZ) marker Brp-short^{cherry} in DA1-PNs only (Schmid et al., 2008, Kremer et al., 2010). The postsynaptic densities (PSDs) of KC dendrites were decorated by cell-type specific expression of GFP-tagged Dα7 subunit of the acetylcholine receptor

(Kremer et al., 2010). We developed a software-based automated 3D-reconstruction tool to identify the MGs exploiting the *MB247-Da7::GFP* signal and classified them as DA1-PN positive if they additionally displayed Brp-short^{cherry} co-labelling (DA1-MG; Figure 1G; Figure S1). Further, we established a standard appetitive associative conditioning paradigm using cVA or geranyl acetate (GA) as CS in STM or LTM paradigms (Figure 2A; Figure S2A–C; see STAR Methods) and applied it to flies expressing the reporters described above (Figure 2B, F, J). Alternatively, we mock-trained the flies by presenting odors and sugar reward separately to avoid the formation of appetitive association (Figure 2A, B, F, J, (Tempel et al., 1983). GA was chosen as it activates a separate and non-overlapping set of PNs in comparison to cVA (Bhandawat et al., 2007) and 5% EtOH was added to both odors to provide a food-related context to the starved flies (Lebreton et al., 2015, Pohl et al., 2012), which was essential to elicit STM (Figure S2B). To assess if MGs formed by DA1-PN boutons (DA1-MGs) underwent morphological modifications after learning, we prepared for confocal imaging female fly brains dissected at 1 min (STM) or at 24 h (LTM) after training. After STM establishment (Figure 2B) the total number, MG volume and lumen volume of DA1-MGs was unchanged in cVA conditioned (cVA CS+) flies compared to the GA conditioned (GA CS+) or mock control groups (average MG numbers: mock 28.91; GA CS+ 30.40; cVA CS+ 28.76; n= 10–17; Figure 2C–E). However, in the LTM paradigm (Figure 2F) the DA1-MGs total volume and lumen volume were decreased in cVA CS+ flies compared to GA CS+ or to mock-control flies (Figure 2G, H). In addition, the total number of DA1-MGs was increased (average MG numbers: mock 27.31; GA CS+ 27.47; cVA CS+ 32.06; n= 18–32; Figure 2I). Thus, LTM, but not STM, was accompanied by an input-specific structural reorganization of the MBC circuit, including an increase in MG number. These changes were specific to the conditioned odor, as they did not appear in the DA1-MGs when the conditioned odor was GA. These data suggest that the neurons delivering the CS form new boutons, which are of smaller size and enveloped by KC claws.

Olfactory associative learning relies on the function of the Ca^{2+}/CaM-dependent adenylyl cyclase Rutabaga (Tempel et al., 1983, Levin et al., 1992, Thum et al., 2007) and a defining trait of LTM is its dependence on protein synthesis (Lagasse et al., 2009, Tully et al., 1994, Davis, 2011). Indeed, a mutation in the *rutabaga* gene (*rut*^{2080}(Han et al., 1992) or feeding flies with the protein synthesis inhibitor cycloheximide (CHX) immediately after training abolished LTM (Figure 2J; Figure S2D). Importantly, loss of *rut* function or CHX feeding also suppressed the structural changes in the DA1-MGs supporting the correlation between LTM formation and structural changes in the circuit (Figure 2K–M; Figure S2E–G).

The increase in DA1-PN positive MG number after LTM formation with cVA CS+ suggests that new boutons might be formed during consolidation. To gain insight into the cellular fundamentals of these modifications, we expressed the membrane-tagged fluorescent protein *UAS-GAP43::Venus* in DA1-PN axons together with *UAS-brp-short*^{cherry} and highlighted the postsynaptic densities on KC dendrites using *MB247-Da7::GFP* (Figure 3A–D). Serial optical sections of the MBCs of these flies trained with cVA CS+, with GA CS+ or in the mock paradigm (Figure S2H) were used to generate 3D reconstructions that were then aligned to a reference brain (JFRC2, (Jenett et al., 2012). The DA1-PN axons were then traced in the aligned high-resolution scans of the MBC (Figure 3E). The DA1-PN boutons were highly clustered in the dorsal-posterior part of the calyx (Clark and Evans, 1954),

supporting the view that the localization of DA1-PN boutons within the MBC is not entirely random (Figure 3F, (Jefferis et al., 2007). The total length of DA1-PN collaterals measured from the point where they leave the inner antennocerebral tract (iACT) was increased in flies that had formed LTM after cVA CS+ training compared to mock-control flies (Figure 3G). In addition, the total volume within the MBC containing DA1-PN positive boutons was increased in flies that had formed cVA CS+ LTM (Figure 3H). These observations suggest that during consolidation, additional boutons are created by local growth at existing DA1-PN collaterals (Figure 3I).

Altered functional response in calycal microglomeruli upon memory consolidation

To address whether the observed structural changes within the MGs after LTM impact on the functional representation of the CS in the MBC we analysed calcium dynamics in KC dendrites. For this, we utilized flies carrying *MB247-homer::GCaMP3* (Pech et al., 2015) in combination with volumetric calcium imaging (Figure 4A). We used this simple genotype to guarantee that flies performed well in LTM experiments (Figure S2I). We measured calcium response in the entire MBC volume during a single odor application (5 s odor stimulation) of either cVA (1:400 in 5% EtOH) or EtOH alone (5%). To identify areas with increased calcium dynamics during odor stimulation we overlaid a grid consisting of 5×5 μm^2 ROIs over each optical section of the volumetric time series. Based on the grid segmentation, we then calculated the average ΔF/F% for each ROI in the MBC. ROIs were classified as odor responsive if the measured calcium response exceeded a set threshold (ΔF/F% > 3x standard deviation, see STAR Methods) during the first 2 s of stimulation (Figure 4B, C; Figure S3A, B). The response pattern elicited specifically by cVA was defined after subtraction of the EtOH response (Figure 4C; Figure S3C, D; see also Figure 1C and STAR Methods). After appetitive LTM formation, the percentage of cVA-responsive ROIs was increased in cVA CS+ flies compared to the mock control (Figure 4D, $n = 7$, $p < 0.05$), suggesting that the additional DA1-PN boutons are functionally connected to their postsynaptic KC counterparts and are capable of initiating a response in the postsynaptic KCs. Linear regression analysis of the fluorescence change over time during odor stimulation showed a steeper drop of the linear fit in cVA CS+ flies ($R^2 = 0.6429$) towards baseline compared to flies of the mock control group ($R^2 = 0.1124$) (Figure 4E, F). Besides, the response towards the odor was more variable in mock-trained flies compared to the cVA CS+ flies (Figure S3F). Initially (0–4s after start of stimulation), the total response towards cVA stimulation was indistinguishable between mock control and cVA CS+ group. However, at subsequent time points (4–7s after start of stimulation) responses were significantly lower in KC dendrites of the cVA CS+ group compared to the mock control, showing a faster calcium decay towards the trained odor in CS+ flies ($n = 7$, $p < 0.05$) (Figure S3G). Together, these data indicate a temporal sharpening of the odor response.

Discussion

We report input-specific reorganization of the adult MBC circuit associated with the formation of long-term appetitive memory. By visualizing presynaptic markers in PNs and the KC postsynaptic densities, we uncover an increase in the number of PN boutons and at the same time reveal that these boutons are enveloped by KC postsynaptic profiles,

suggesting that new MGs are formed during memory consolidation. These findings are particularly remarkable, given the high degree of complexity of the MG microcircuits revealed by our EM reconstruction and including the dendrite claws of multiple KCs of distinct subtypes. The cellular mechanisms leading to the increased number of odor-specific complex MGs remain to be clarified, but they will require a tight coordination between pre- and postsynaptic partners. In this context, mutations in synaptic proteins or in proteins mediating cell- cell interactions that specifically block LTM will be of great interest (Silva et al., 2020, Gouzi et al., 2018). We suggest that remodelling could be driven by intrinsic reactivation of KCs during the consolidation phase (Ichinose et al., 2015, Cognigni et al., 2018) or by modulatory inputs into the calyx (Mao and Davis, 2009, Chen et al., 2012, Aso et al., 2014, Busch et al., 2009, Boto et al., 2019). In either case, we expect a complex pattern of activation that might be difficult to reproduce in artificial settings (Kremer et al., 2010, Warth Perez Arias et al., 2020). While our present observations are limited for technical reasons to the specific case of cVA, the overall density of PN boutons in the MBC increases after appetitive long-term conditioning in honeybees as well as in leaf-cutting ants after avoidance learning (Hourcade et al., 2010, Falibene et al., 2015). Based on this, and given that the olfactory pathway of cVA is not distinguishable from that of other odors, we thus suggest that our findings might be generalizable. In comparison to those systems though, we use genetic and functional identification of PN subsets to reveal that the structural modifications are specific and limited to the PNs conveying the conditioned odor. Importantly, our *in vivo* functional imaging data support the view that the circuit reorganization leads to additional functional MGs responding to the conditioned odor. Additionally, they demonstrate a specific change in functional response in the KC dendrites towards the trained odor as the calcium levels drop faster towards baseline after appetitive associative conditioning. The faster decay kinetics and more skewed response towards the onset of the stimulus could contribute to a more efficient temporal summation of responses or refine the KC response and might be related to inhibitory modifications (Gupta and Stopfer, 2014, Haenicke et al., 2018). An important open question is the effect of the increased number of responding MGs on the pattern of KC activation. KCs respond sparsely to odor input and require the coincident activation of multiple of their claws to produce an action potential (Gruntman and Turner, 2013). Our data might underlie the addition of connections between the active PNs and a set of already responding KCs, leading to facilitated response to the conditioned odor without changing the set of responding KCs. A recent publication, however, suggests an exciting alternative view. After aversive LTM establishment, the number of KCs responding to the conditioned odor is increased (Delestro et al., 2020). If we hypothesize that appetitive conditioning leads to a similar outcome, our data could provide anatomical and functional support to these findings. The pattern of KC response could thus be modulated by experience in adulthood and might represent a rich signifier of sensory stimulus and context.

STAR Methods

RESOURCE AVAILABILITY

Lead Contact—Further information and requests for resources and reagents should be directed to and will be fulfilled by the Lead Contact, Gaia Tavosanis (gaia.tavosanis@dzne.de)

Materials Availability—All stable reagents generated in this study are available from the Lead Contact upon request.

Data and code availability—The electron microscopy dataset analysed in this study was generated in (Zheng et al., 2018).

The Definiens™ script used in this study for microglomeruli detection and analysis is available from the Lead Contact on request.

EXPERIMENTAL MODEL AND SUBJECT DETAILS

Flies were raised at 25°C, 60% relative humidity in a 12h/12h light-dark cycle on a standard cornmeal-based diet and collected 0–4d after eclosion for experiments. Behavioral experiments were performed on mixed populations of female and male adult flies. Brains of adult females were dissected for immunohistochemistry and calcium imaging experiments. The fly stocks used in this work were *R37H08-Gal4* (Kind gift of Y. Aso, HHMI, Janelia), *P{UASp-Venus.GAP43}10* (Bloomington Drosophila Stock center), *P{UAS-tdTom.S}2* (Bloomington Drosophila Stock center), *P{ry[+t7.2]=IArB}rut[2080]* (Han et al., 1992), *P{UAS-GCaMP3.homer}* (Pech et al., 2015), *MB247-Dα7::GFP* (Kremer et al., 2010) and *UAS-brp-short*^{cherry} (Kremer et al., 2010).

METHOD DETAILS

Behaviour—All experimental steps were performed at 23°C, 60% relative humidity using mixed populations of *Drosophila* males and females maintained in a 12h/12h light/dark cycle. Flies were collected 0–4d after eclosion, starved for 24 hours on wet paper tissue (Kimberly-Clark Worldwide Inc.) allowing for water uptake and then trained. In appetitive memory experiments ~80 flies were first exposed to an odor (CS−) alone (2min in short- and 5 minutes in long-term memory experiments). After a 2min inter-stimulus pause flies were trained by receiving dry sucrose on filter paper (3M Chr, Whatman) paired with a second odor (CS+) (2min in short- and 5 minutes in long-term memory experiments). 5 minutes of sugar availability improved the survival of flies undergoing the LTM paradigm. In mock controls, all stimuli used in the associative conditioning experiment were presented separately. Flies were tested after 1min retention time for short- or after 24h retention time for long-term memory. During the 24h retention flies were deprived of food and maintained in tubes containing moist paper tissue. During the test flies were allowed to choose between CS+ and CS− odors in a T-maze for 2min. Odors used for conditioning were 11-cis vaccenyl acetate (Cayman Chemicals) 1:400 in 5% EtOH in PBS, geranyl acetate (Sigma Aldrich) 1:100 in 5% EtOH in PBS or 5% EtOH in PBS. EtOH was necessary to provide a food-related context to the starved flies (Figure S2B).

De-novo protein synthesis inhibition—Immediately after training, flies were fed 35 mM cycloheximide (Sigma-Aldrich) (Tully et al., 1994) dissolved in 125mM sucrose and 0.01% carmine solution for 30min. The red dye carmine allowed confirming rapid drug uptake. A control group fed with 125mM sucrose and 0.01% carmine (Sigma-Aldrich) solution showed no learning defects.

Immunohistochemistry—2–5 flies were randomly picked from conditioning experiments right before testing. Brains of females were dissected in cold phosphate-buffered saline (PBS) with 0.05% Triton and subsequently fixed in PBS containing 4% formaldehyde at RT for 50 min. After fixation brains were washed in PBS with 0.3% Triton before incubation overnight at 4°C with the following primary antibodies all diluted in PBS with 0.3% Triton: rabbit anti-RFP (1:2000; Rockland), rabbit anti-GFP (1:200; Life Technologies), mouse monoclonal anti-synapsin (3C11, 1:100; DSHB), mouse monoclonal anti-β-Galactosidase (1:200 Abcam). After washing, the brains were incubated with secondary antibodies in PBS containing 0.3% Triton for 4h at RT. The secondary antibodies were Alexa Fluor568-conjugated goat anti-rabbit, Alexa Fluor488-conjugated goat anti-rabbit, Alexa Fluor568-conjugated goat anti-mouse, Alexa Fluor633-conjugated goat anti-mouse (all used 1:200 and from Life Technologies). Brains were mounted in Vectashield (Vector) and imaged with a laser scanning confocal microscope (LSM 780, Zeiss). For high resolution scans we used a C Plan-Apochromat 63x/1,4 Oil objective (Zeiss) with a voxel size of $0.09\times0.09\times0.25\mu m^3$ for quantitative analysis. Overviews of entire brains were taken with an LCI Plan-Apochromat 25x/0.8 objective (Zeiss) at a voxel size of $0.55\times0.55\times1\mu m^3$.

To analyse axon and bouton distribution in the calyx, membrane-tagged Venus was expressed in addition to the previously used markers under the control of a DA1-PN Gal4-driver line (*R37H08-GAL4, UAS-Gap43::Venus / MB247-Dα7::GFP, UAS-brp-short*^{cherry}). Brains of 10 female flies per condition were immunolabelled with anti-synapsin antibodies (as above) and imaged. For PN axon reconstruction a high-resolution scan ($0.09\times0.09\times0.25\mu m^3$, 63x NA1.4 oil immersion) of the right brain hemisphere of female flies was acquired with a confocal microscope. In addition, an overview scan used for registration was taken with a low magnification objective (25x; NA 0.8 multi-immersion).

Two-photon *in vivo* calcium imaging—A mixed population of up to 4d old *MB247-homer::GCaMP3* flies were starved for 18h at 22°C before appetitive conditioning with cVA (1:400, 5% EtOH in PBS), GA (1:100, 5% EtOH in PBS) was used as CS−. Starved untrained flies displayed no bias towards either of these odors at 24 hours. Flies used for imaging were randomly picked from the trained group right before testing. They were used for imaging only if the remaining flies from the same group had learned. For imaging, flies were briefly anesthetized on a Peltier element at 4°C, placed into a custom-built imaging chamber (Figure 4A) and fixed using adhesive tape. The head capsule was opened under Ringeŕs solution (5 mM HEPES, pH 7.4, 130 mM NaCl, 5 mM KCl, 2 mM $CaCl_2$, 2 mM $MgCl_2$). To minimize movement brains were stabilized with 1,5% low melting agarose (Thermo Scientific) in Ringeŕs solution. Flies were imaged with a two-photon laser-scanning microscope (LaVision BioTec, TriM Scope II) equipped with an ultra-fast

z-motor (PIFOC® Objective Scanner Systems 100μm range) and a Zeiss C-Apochromat 40x, 1.1 NA water –immersion objective. Two-photon images were analysed using Fiji/ImageJ (Schindelin et al., 2012). GCaMP fluorescence was excited at 920 nm using a Ti:sapphire laser (Coherent Chameleon). A stack consisting of ~ 10 optical sections was taken at 1Hz in approximately 0,26×0,26μm xy- and at 4μm z- resolution. Odors were applied with a constant humidified air stream (10ml/s) using a commercial device (Stimulus Controller CS 55, Ockenfels SYNTECH GbmH) triggered 5s after acquisition of the 1st frame by a multifunction I/O module (NI USB-6008), which was controlled by Matlab (Data Acquisition Toolbox). To record DA1 neurons specific responses, *UAS-tdTomato; R37H08-GAL4, MB247-Homer::GCaMP3* flies were anesthetized on ice, positioned in a polycarbonate imaging chamber ((Louis et al., 2018), and immobilized using Myristic Acid (Sigma-Aldrich). To allow optical access to the Calyx, a small window was opened through the head capsule under Ringeŕs solution. Two-photon microscopy was conducted as described above.

QUANTIFICATION AND STATISTICAL ANALYSIS

EM reconstruction and identification—Neuron skeletons were reconstructed in a serial section transmission electron microscope (ssTEM) volume of a complete female adult *Drosophila melanogaster* brain (Zheng et al., 2018) and manually traced using CATMAID (Saalfeld et al., 2009). Thus, traced neuron skeletons represent the branching of neurons and the location of their cell bodies and synapses. Chemical synapses were manually annotated and identified consistently with the criteria of other CATMAID-based *Drosophila* connectomic studies (Zheng et al., 2018): 1) an active zone (AZ) surrounded by vesicles, 2) a presynaptic specialization (*e.g.* T-bar), 3) synaptic cleft and 4) a post synaptic density zone (PSD), which however can be absent. If the PSD is absent, we annotated all cells along the synaptic cleft as postsynaptic (Zheng et al., 2018, Prokop and Meinertzhagen, 2006). Neuron identity is based on previously described morphologies in light microscopy (KC subtypes, APL, MB-C1, PN), such as dendritic branching, axonal projection and location in the neuropil (Aso et al., 2014, Tanaka et al., 2008, Liu and Davis, 2009, Grabe et al., 2015, Jefferis et al., 2007). Additionally, we performed a neuron search against a light microscopy dataset in NBLAST (Costa et al., 2016), as described in (Zheng et al., 2018) for PN subtype identification. 3D reconstructions of the PN bouton and KC claws from ssTEM sections were created manually with the ImageJ plugin TrakEM2 (Cardona et al., 2012).

Behaviour—A performance index (PI) was calculated as the ratio of the difference between the number of flies that chose the CS+ and those that chose the CS− odor and the total number of flies: $PI = \frac{(CS+) - (CS-)}{(CS+) + (CS-)}$.

Axon Reconstruction—PN axon reconstruction was performed on the high-resolution scan of Venus signal in the trees toolbox available for Matlab (Cuntz et al., 2010). In a second step, tracings and high-resolution images were aligned to the registered calyx. For generation of a standard calyx with a volume of 37583 μm^3 (Figure 3E, light green) the Dα7 signal of three registered calyces was averaged and reconstructed in Amira using the segmentation editor. Next, tracings were aligned to the registered overview scan in two

steps. First, the iACT of the high-resolution image and of the registered brain in the Venus channel were aligned. Next, the calyx volume of the high-resolution calyx and the standard calyx went through a rigid registration performed in Amira. The alignment parameters were then applied to the axon reconstructions. Boutons were traced on the now registered high-resolution images with the landmark function in Amira. Bouton distribution inside the MBC was evaluated within a 3D grid of 10μm^3 cubes.

Two-photon image data processing—The time series was processed with a custom Fiji/ ImageJ macro and corrected for small x/y shifts with the StackReg plug-in (Thevenaz et al., 1998). A grid (ROIs, side length 5 μm) was assigned for each optical slide of a stack covering the entire calyx. Intensity tables of each square of the grid were exported to Microsoft Excel and the ΔF/F was calculated. The baseline (F_0) was set by averaging the intensities within each ROI of the 5 frames prior to odor stimulation. ROIs were regarded as responsive, if their normalized ΔF/F% throughout the first 2s of odor application exceeded 3x the standard deviation of the F_0 of the same ROI in the 5s (=5 images) before odor stimulation. The 3x standard deviation threshold was chosen as it provided the suitable sensitivity for the evaluation of odor-elicited responses without introducing excessive noise. ROIs below that threshold were assigned into the category “unresponsive”. ROIs calcium responses higher than the threshold were further subdivided into three categories. The first category was “Carrier” (responsive to both, 5% EtOH and 1:400 cVA, 5% EtOH). The second category was “cVA” (responsive only to 1:400 cVA, 5% EtOH and not to 5% EtOH) or “EtOH” (response only to 5% EtOH application and not to 1:400 cVA, 5% EtOH). To analyse DA1 boutons responses to 5% EtOH and 1:400 cVA+ 5% EtOH were recorded from naïve *UAS-tdTomato; R37H08-GAL4, MB247-Homer::GCaMP3* flies, exported to Fiji/ImageJ and ROIs were manually drawn around DA1 boutons based on the tdTomato fluorescence. Intensity values of each ROI were transferred to Microsoft Excel and ΔF/F values were calculated using the average of the first 5 frames prior to odor stimulation as baseline (F_0). Responsive ROIs were defined as above. These results were age, gender and sequence independent as presenting the odors in a different order did not change the results of the analysis. Calcium traces were generated in Prism 7 (GraphPad Software).

Statistics—Statistical analyses were performed with Prism7.01 software (GraphPad). All data were tested for normality (D’Agostino & Pearson omnibus normality test) and homogeneity of variances (F-test). Comparisons of normally distributed data were tested by a one-sample t test, a two-sample t test or one-way analysis of variance (ANOVA) followed by planned, pairwise multiple-comparison tests with adjusted p-values (Bonferroni). Definition of statistical significance was set to <0.05. Asterisks denote * p<0.05; ** p<0.01; ***p<0.001; **** p<0.0001; n.s. not significant. All experimental tests performed and their relative p-values are reported in Supplementary Table 2.

Supplementary Material

Refer to Web version on PubMed Central for supplementary material.

Acknowledgements

We thank LMF and IDAF at DZNE, A. Mueller, R. Kerpen and J. C. Vijayakumar for technical assistance. We are grateful to C.B. Fisher, S.A. Calle-Schuler, N. Sharifi, B. Gorko, L. Kmecova, I.J. Ali, N. Masoodpanah, J. Hsu and F. Li in D. D. Bock's lab for their support in tracing evaluation. We thank Y. Aso, HHMI Janelia, the Kyoto Drosophila Genetic Resource Center and the Bloomington Stock Center for fly lines and FlyBase. We are grateful for their assistance to DZNE IDAF in the establishment of the cluster analysis, S. Dipt with initial calcium imaging experiments and R. Court for providing the brain aligner and support. We thank S. Sachse, D. Isbrandt, T. Hige, S. Remy, M. Nawrot, O. Barnstedt, the members of the Tavosanis lab for discussion and/or critical reading of the manuscript and B. Schaffran for help with video editing. L.B. acknowledges support by the Bonn International Graduate School of Neuroscience. This work was supported by the DFG FOR 2705 to G.T.

References

ASO Y, HATTORI D, YU Y, JOHNSTON RM, IYER NA, NGO TT, DIONNE H, ABBOTT LF, AXEL R, TANIMOTO H & RUBIN GM 2014. The neuronal architecture of the mushroom body provides a logic for associative learning. Elife, 3, e04577. [PubMed: 25535793]

BAILEY CH, BARTSCH D & KANDEL ER 1996. Toward a molecular definition of long-term memory storage. Proc Natl Acad Sci U S A, 93, 13445–52. [PubMed: 8942955]

BASSETT DS, WYMBS NF, PORTER MA, MUCHA PJ, CARLSON JM & GRAFTON ST 2011. Dynamic reconfiguration of human brain networks during learning. Proc Natl Acad Sci U S A, 108, 7641–6. [PubMed: 21502525]

BENNETT SH, KIRBY AJ & FINNERTY GT 2018. Rewiring the connectome: Evidence and effects. Neurosci Biobehav Rev, 88, 51–62. [PubMed: 29540321]

BHANDAWAT V, OLSEN SR, GOUWENS NW, SCHLIEF ML & WILSON RI 2007. Sensory processing in the Drosophila antennal lobe increases reliability and separability of ensemble odor representations. Nat Neurosci, 10, 1474–82. [PubMed: 17922008]

BOELE HJ, KOEKKOEK SK, DE ZEEUW CI & RUIGROK TJ 2013. Axonal sprouting and formation of terminals in the adult cerebellum during associative motor learning. J Neurosci, 33, 17897–907. [PubMed: 24198378]

BOTO T, STAHL A & TOMCHIK SM 2020. Cellular and circuit mechanisms of olfactory associative learning in Drosophila. J Neurogenet, 34, 36–46. [PubMed: 32043414]

BOTO T, STAHL A, ZHANG X, LOUIS T & TOMCHIK SM 2019. Independent Contributions of Discrete Dopaminergic Circuits to Cellular Plasticity, Memory Strength, and Valence in Drosophila. Cell Rep, 27, 2014–2021 e2. [PubMed: 31091441]

BURKE CJ, HUETTEROTH W, OWALD D, PERISSE E, KRASHES MJ, DAS G, GOHL D, SILIES M, CERTEL S & WADDELL S 2012. Layered reward signalling through octopamine and dopamine in Drosophila. Nature, 492, 433–7. [PubMed: 23103875]

BUSCH S, SELCHO M, ITO K & TANIMOTO H 2009. A map of octopaminergic neurons in the Drosophila brain. J Comp Neurol, 513, 643–67. [PubMed: 19235225]

BUTCHER NJ, FRIEDRICH AB, LU Z, TANIMOTO H & MEINERTZHAGEN IA 2012. Different classes of input and output neurons reveal new features in microglomeruli of the adult Drosophila mushroom body calyx. J Comp Neurol, 520, 2185–201. [PubMed: 22237598]

CARDONA A, SAALFELD S, SCHINDELIN J, ARGANDA-CARRERAS I, PREIBISCH S, LONGAIR M, TOMANCAK P, HARTENSTEIN V & DOUGLAS RJ 2012. TrakEM2 software for neural circuit reconstruction. PLoS One, 7, e38011. [PubMed: 22723842]

CARON SJ, RUTA V, ABBOTT LF & AXEL R 2013. Random convergence of olfactory inputs in the Drosophila mushroom body. Nature, 497, 113–7. [PubMed: 23615618]

CARONI P, DONATO F & MULLER D 2012. Structural plasticity upon learning: regulation and functions. Nat Rev Neurosci, 13, 478–90. [PubMed: 22714019]

CERVANTES-SANDOVAL I, MARTIN-PENA A, BERRY JA & DAVIS RL 2013. System-like consolidation of olfactory memories in Drosophila. J Neurosci, 33, 9846–54. [PubMed: 23739981]

CHEN CC, WU JK, LIN HW, PAI TP, FU TF, WU CL, TULLY T & CHIANG AS 2012. Visualizing long-term memory formation in two neurons of the Drosophila brain. Science, 335, 678–85. [PubMed: 22323813]

CHEN JL, MARGOLIS DJ, STANKOV A, SUMANOVSKI LT, SCHNEIDER BL & HELMCHEN F 2015. Pathway-specific reorganization of projection neurons in somatosensory cortex during learning. Nat Neurosci, 18, 1101–8. [PubMed: 26098757]

CHKLOVSKII DB, MEL BW & SVOBODA K 2004. Cortical rewiring and information storage. Nature, 431, 782–8. [PubMed: 15483599]

CLARK PJ & EVANS FC 1954. Distance to nearest neighbour as a measure of spatial relationships in populations. Ecology 35, 445–453.

COGNIGNI P, FELSENBERG J & WADDELL S 2018. Do the right thing: neural network mechanisms of memory formation, expression and update in Drosophila. Curr Opin Neurobiol, 49, 51–58. [PubMed: 29258011]

COSTA M, MANTON JD, OSTROVSKY AD, PROHASKA S & JEFFERIS GS 2016. NBLAST: Rapid, Sensitive Comparison of Neuronal Structure and Construction of Neuron Family Databases. Neuron, 91, 293–311. [PubMed: 27373836]

CUNTZ H, FORSTNER F, BORST A & HAUSSER M 2010. One rule to grow them all: a general theory of neuronal branching and its practical application. PLoS Comput Biol, 6.

DATTA SR, VASCONCELOS ML, RUTA V, LUO S, WONG A, DEMIR E, FLORES J, BALONZE K, DICKSON BJ & AXEL R 2008. The Drosophila pheromone cVA activates a sexually dimorphic neural circuit. Nature, 452, 473–7. [PubMed: 18305480]

DAVIS RL 2011. Traces of Drosophila memory. Neuron, 70, 8–19. [PubMed: 21482352]

DE BELLE JS & HEISENBERG M 1994. Associative odor learning in Drosophila abolished by chemical ablation of mushroom bodies. Science, 263, 692–5. [PubMed: 8303280]

DELESTRO F, SCHEUNEMANN L, PEDRAZZANI M, TCHENIO P, PREAT T & GENOVESIO A 2020. In vivo large-scale analysis of Drosophila neuronal calcium traces by automated tracking of single somata. Scientific Reports, 10, 7153. [PubMed: 32346011]

DUBNAU J & CHIANG AS 2013. Systems memory consolidation in Drosophila. Curr Opin Neurobiol, 23, 84–91. [PubMed: 23084099]

FALIBENE A, ROCES F & ROSSLER W 2015. Long-term avoidance memory formation is associated with a transient increase in mushroom body synaptic complexes in leaf-cutting ants. Front Behav Neurosci, 9, 84. [PubMed: 25904854]

GOGOLLA N, GALIMBERTI I & CARONI P 2007. Structural plasticity of axon terminals in the adult. Curr Opin Neurobiol, 17, 516–24. [PubMed: 17950593]

GOUZI JY, BOURAIMI M, ROUSSOU IG, MORESSIS A & SKOULAKIS EMC 2018. The Drosophila Receptor Tyrosine Kinase Alk Constrains Long-Term Memory Formation. J Neurosci, 38, 7701–7712. [PubMed: 30030398]

GRABE V, STRUTZ A, BASCHWITZ A, HANSSON BS & SACHSE S 2015. Digital in vivo 3D atlas of the antennal lobe of Drosophila melanogaster. J Comp Neurol, 523, 530–44. [PubMed: 25327641]

GREWE BF, GRUNDEMANN J, KITCH LJ, LECOQ JA, PARKER JG, MARSHALL JD, LARKIN MC, JERCOG PE, GRENIER F, LI JZ, LUTHI A & SCHNITZER MJ 2017. Neural ensemble dynamics underlying a long-term associative memory. Nature, 543, 670–675. [PubMed: 28329757]

GRUNTMAN E & TURNER GC 2013. Integration of the olfactory code across dendritic claws of single mushroom body neurons. Nat Neurosci, 16, 1821–9. [PubMed: 24141312]

GU S, PASQUALETTI F, CIESLAK M, TELESFORD QK, YU AB, KAHN AE, MEDAGLIA JD, VETTEL JM, MILLER MB, GRAFTON ST & BASSETT DS 2015. Controllability of structural brain networks. Nat Commun, 6, 8414. [PubMed: 26423222]

GUPTA N & STOPFER M 2014. A temporal channel for information in sparse sensory coding. Curr Biol, 24, 2247–56. [PubMed: 25264257]

HAENICKE J, YAMAGATA N, ZWAKA H, NAWROT M & MENZEL R 2018. Neural Correlates of Odor Learning in the Presynaptic Microglomerular Circuitry in the Honeybee Mushroom Body Calyx. eNeuro, 5.

HAN PL, LEVIN LR, REED RR & DAVIS RL 1992. Preferential expression of the Drosophila rutabaga gene in mushroom bodies, neural centers for learning in insects. Neuron, 9, 619–27. [PubMed: 1382471]

HIHARA S, NOTOYA T, TANAKA M, ICHINOSE S, OJIMA H, OBAYASHI S, FUJII N & IRIKI A 2006. Extension of corticocortical afferents into the anterior bank of the intraparietal sulcus by tool-use training in adult monkeys. Neuropsychologia, 44, 2636–46. [PubMed: 16427666]

HOLTMAAT A & CARONI P 2016. Functional and structural underpinnings of neuronal assembly formation in learning. Nat Neurosci, 19, 1553–1562. [PubMed: 27749830]

HOURCADE B, MUENZ TS, SANDOZ JC, ROSSLER W & DEVAUD JM 2010. Long-term memory leads to synaptic reorganization in the mushroom bodies: a memory trace in the insect brain? J Neurosci, 30, 6461–5. [PubMed: 20445072]

ICHINOSE T, ASO Y, YAMAGATA N, ABE A, RUBIN GM & TANIMOTO H 2015. Reward signal in a recurrent circuit drives appetitive long-term memory formation. Elife, 4, e10719. [PubMed: 26573957]

JEFFERIS GS, POTTER CJ, CHAN AM, MARIN EC, ROHLFING T, MAURER CR JR. & LUO L 2007. Comprehensive maps of Drosophila higher olfactory centers: spatially segregated fruit and pheromone representation. Cell, 128, 1187–203. [PubMed: 17382886]

JENETT A, RUBIN GM, NGO TT, SHEPHERD D, MURPHY C, DIONNE H, PFEIFFER BD, CAVALLARO A, HALL D, JETER J, IYER N, FETTER D, HAUSENFLUCK JH, PENG H, TRAUTMAN ET, SVIRSKAS RR, MYERS EW, IWINSKI ZR, ASO Y, DEPASQUALE GM, ENOS A, HULAMM P, LAM SC, LI HH, LAVERTY TR, LONG F, QU L, MURPHY SD, ROKICKI K, SAFFORD T, SHAW K, SIMPSON JH, SOWELL A, TAE S, YU Y & ZUGATES CT 2012. A GAL4-driver line resource for Drosophila neurobiology. Cell Rep, 2, 991–1001. [PubMed: 23063364]

JOSSELYN SA & TONEGAWA S 2020. Memory engrams: Recalling the past and imagining the future. Science, 367.

KITAMURA T & OGAWA SK 2017. Engrams and circuits crucial for systems consolidation of a memory. 356, 73–78.

KLEIM JA, FREEMAN JH JR., BRUNEAU R, NOLAN BC, COOPER NR, ZOOK A & WALTERS D 2002. Synapse formation is associated with memory storage in the cerebellum. Proc Natl Acad Sci U S A, 99, 13228–31. [PubMed: 12235373]

KREMER MC, CHRISTIANSEN F, LEISS F, PAEHLER M, KNAPEK S, ANDLAUER TF, FORSTNER F, KLOPPENBURG P, SIGRIST SJ & TAVOSANIS G 2010. Structural long-term changes at mushroom body input synapses. Curr Biol, 20, 1938–44. [PubMed: 20951043]

KURTOVIC A, WIDMER A & DICKSON BJ 2007. A single class of olfactory neurons mediates behavioural responses to a Drosophila sex pheromone. Nature, 446, 542–6. [PubMed: 17392786]

LAGASSE F, DEVAUD JM & MERY F 2009. A switch from cycloheximide-resistant consolidated memory to cycloheximide-sensitive reconsolidation and extinction in Drosophila. J Neurosci, 29, 2225–30. [PubMed: 19228975]

LEBRETON S, GRABE V, OMONDI AB, IGNELL R, BECHER PG, HANSSON BS, SACHSE S & WITZGALL P 2014. Love makes smell blind: mating suppresses pheromone attraction in Drosophila females via Or65a olfactory neurons. Sci Rep, 4, 7119. [PubMed: 25406576]

LEBRETON S, TRONA F, BORRERO-ECHEVERRY F, BILZ F, GRABE V, BECHER PG, CARLSSON MA, NÄSSEL DR, HANSSON BS, SACHSE S & WITZGALL P 2015. Feeding regulates sex pheromone attraction and courtship in Drosophila females. Scientific Reports, 5, 13132. [PubMed: 26255707]

LEISS F, GROH C, BUTCHER NJ, MEINERTZHAGEN IA & TAVOSANIS G 2009. Synaptic organization in the adult Drosophila mushroom body calyx. J Comp Neurol, 517, 808–24. [PubMed: 19844895]

LEVIN LR, HAN PL, HWANG PM, FEINSTEIN PG, DAVIS RL & REED RR 1992. The Drosophila learning and memory gene rutabaga encodes a Ca2+/Calmodulin-responsive adenylyl cyclase. Cell, 68, 479–89. [PubMed: 1739965]

LIN HH, LAI JS, CHIN AL, CHEN YC & CHIANG AS 2007. A map of olfactory representation in the Drosophila mushroom body. Cell, 128, 1205–17. [PubMed: 17382887]

LIU C, PLACAIS PY, YAMAGATA N, PFEIFFER BD, ASO Y, FRIEDRICH AB, SIWANOWICZ I, RUBIN GM, PREAT T & TANIMOTO H 2012. A subset of dopamine neurons signals reward for odor memory in Drosophila. Nature, 488, 512–6. [PubMed: 22810589]

LIU X & DAVIS RL 2009. The GABAergic anterior paired lateral neuron suppresses and is suppressed by olfactory learning. Nat Neurosci, 12, 53–9. [PubMed: 19043409]

LOUIS T, STAHL A, BOTO T & TOMCHIK SM 2018. Cyclic AMP-dependent plasticity underlies rapid changes in odor coding associated with reward learning. Proc Natl Acad Sci U S A, 115, E448–E457. [PubMed: 29284750]

MAO Z & DAVIS RL 2009. Eight different types of dopaminergic neurons innervate the Drosophila mushroom body neuropil: anatomical and physiological heterogeneity. Front Neural Circuits, 3, 5. [PubMed: 19597562]

MAVIEL T, DURKIN TP, MENZAGHI F & BONTEMPI B 2004. Sites of neocortical reorganization critical for remote spatial memory. Science (New York, N.Y.), 305, 96–99.

PECH U, REVELO NH, SEITZ KJ, RIZZOLI SO & FIALA A 2015. Optical dissection of experience-dependent pre- and postsynaptic plasticity in the Drosophila brain. Cell Rep, 10, 2083–95. [PubMed: 25818295]

POHL JB, BALDWIN BA, DINH BL, RAHMAN P, SMEREK D, PRADO FJ, SHERAZEE N & ATKINSON NS 2012. Ethanol preference in Drosophila melanogaster is driven by its caloric value. Alcoholism, clinical and experimental research, 36, 1903–1912.

POORT J, KHAN AG, PACHITARIU M, NEMRI A, ORSOLIC I, KRUPIC J, BAUZA M, SAHANI M, KELLER GB, MRSIC-FLOGEL TD & HOFER SB 2015. Learning Enhances Sensory and Multiple Non-sensory Representations in Primary Visual Cortex. Neuron, 86, 1478–90. [PubMed: 26051421]

PROKOP A & MEINERTZHAGEN IA 2006. Development and structure of synaptic contacts in Drosophila. Semin Cell Dev Biol, 17, 20–30. [PubMed: 16384719]

SAALFELD S, CARDONA A, HARTENSTEIN V & TOMANCAK P 2009. CATMAID: collaborative annotation toolkit for massive amounts of image data. Bioinformatics, 25, 1984–6. [PubMed: 19376822]

SCHINDELIN J, ARGANDA-CARRERAS I, FRISE E, KAYNIG V, LONGAIR M, PIETZSCH T, PREIBISCH S, RUEDEN C, SAALFELD S, SCHMID B, TINEVEZ JY, WHITE DJ, HARTENSTEIN V, ELICEIRI K, TOMANCAK P & CARDONA A 2012. Fiji: an open-source platform for biological-image analysis. Nat Methods, 9, 676–82. [PubMed: 22743772]

SCHLIEF ML & WILSON RI 2007. Olfactory processing and behavior downstream from highly selective receptor neurons. Nat Neurosci, 10, 623–30. [PubMed: 17417635]

SCHMID A, HALLERMANN S, KITTEL RJ, KHORRAMSHAHI O, FROLICH AM, QUENTIN C, RASSE TM, MERTEL S, HECKMANN M & SIGRIST SJ 2008. Activity-dependent site-specific changes of glutamate receptor composition in vivo. Nat Neurosci, 11, 659–66. [PubMed: 18469810]

SILVA B, NIEHAGE C, MAGLIONE M, HOFLACK B, SIGRIST SJ, WASSMER T, PAVLOWSKY A & PREAT T 2020. Interactions between amyloid precursor protein-like (APPL) and MAGUK scaffolding proteins contribute to appetitive long-term memory in Drosophila melanogaster. J Neurogenet, 34, 92–105. [PubMed: 31965876]

TANAKA NK, TANIMOTO H & ITO K 2008. Neuronal assemblies of the Drosophila mushroom body. J Comp Neurol, 508, 711–55. [PubMed: 18395827]

TEMPEL BL, BONINI N, DAWSON DR & QUINN WG 1983. Reward learning in normal and mutant Drosophila. Proc Natl Acad Sci U S A, 80, 1482–6. [PubMed: 6572401]

THEVENAZ P, RUTTIMANN UE & UNSER M 1998. A pyramid approach to subpixel registration based on intensity. IEEE Trans Image Process, 7, 27–41. [PubMed: 18267377]

THUM AS, JENETT A, ITO K, HEISENBERG M & TANIMOTO H 2007. Multiple memory traces for olfactory reward learning in Drosophila. J Neurosci, 27, 11132–8. [PubMed: 17928455]

TULLY T, PREAT T, BOYNTON SC & DEL VECCHIO M 1994. Genetic dissection of consolidated memory in Drosophila. Cell, 79, 35–47. [PubMed: 7923375]

WANG Y, MAMIYA A, CHIANG A-S & ZHONG Y 2008. Imaging of an early memory trace in the Drosophila mushroom body. The Journal of neuroscience : the official journal of the Society for Neuroscience, 28, 4368–4376. [PubMed: 18434515]

WARTH PEREZ ARIAS CC, FROSCH P, FIALA A & RIEMENSPERGER TD 2020. Stochastic and Arbitrarily Generated Input Patterns to the Mushroom Bodies Can Serve as Conditioned Stimuli in Drosophila. Front Physiol, 11, 53. [PubMed: 32116764]

YASUYAMA K, MEINERTZHAGEN IA & SCHURMANN FW 2002. Synaptic organization of the mushroom body calyx in Drosophila melanogaster. J Comp Neurol, 445, 211–26. [PubMed: 11920702]

ZHENG Z, LAURITZEN JS, PERLMAN E, ROBINSON CG, NICHOLS M, MILKIE D, TORRENS O, PRICE J, FISHER CB, SHARIFI N, CALLE-SCHULER SA, KMECOVA L, ALI IJ, KARSH B, TRAUTMAN ET, BOGOVIC JA, HANSLOVSKY P, JEFFERIS G, KAZHDAN M, KHAIRY K, SAALFELD S, FETTER RD & BOCK DD 2018. A Complete Electron Microscopy Volume of the Brain of Adult Drosophila melanogaster. Cell, 174, 730–743 e22. [PubMed: 30033368]

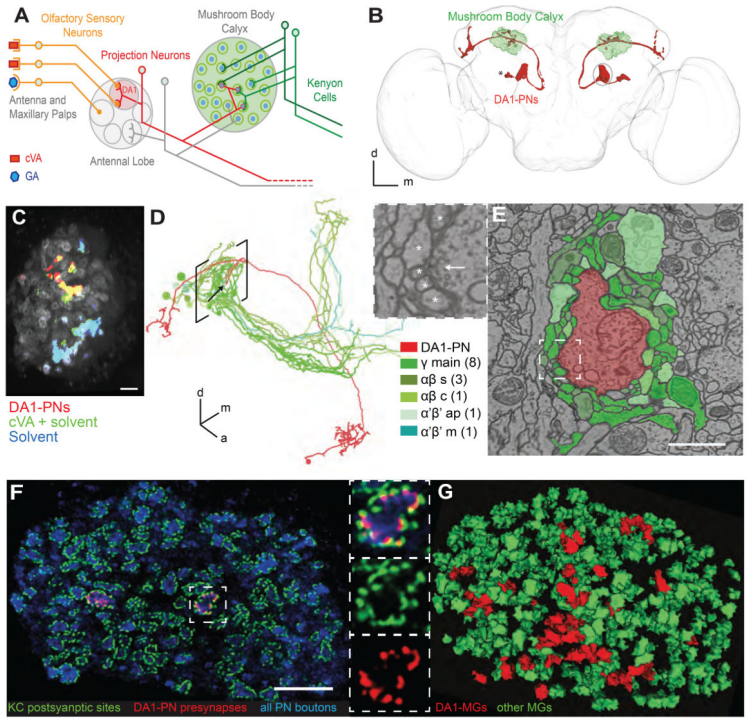

Figure 1 |. Identification of the synapses in the MBC responding to cVA odor stimulation

(A) Schematic representation of the olfactory circuit starting from the activation of specific Olfactory Sensory Neurons (OSNs) by two exemplary odors cVA and GA. In the AL cVA-responsive OSNs converge to the DA1 glomerulus (pale red), where they synapse onto DA1-PNs (red). These deliver the cVA signal to the MBC via axon collaterals that terminate with boutons forming large synaptic complexes, the MGs (circles). Postsynaptic KCs are represented in green. **(B)** Reconstruction from a full confocal serial section set of the DA1-PNs (red; *R37H08-Gal4> UAS GAP43::Venus*); MBC (green; *MB247-Dα7::GFP*); DA1-PN cell bodies (*); brain neuropil (light grey; *α*-synapsin antibody). **(C)** Volumetric calcium imaging of the calyx of flies carrying *MB247-Homer::GCaMP3* (grey) and in which DA1-PNs are genetically labelled (red; *R37H08-Gal4> UAS tdTomato*). cVA-elicited postsynaptic responses (green; cVA 1:400 dissolved in 5% EtOH) are specific to DA1-PNs as revealed by the overlap between the two channels (red + green= yellow). Generic response to the solvent (cyan= overlap of the responses to cVA 1:400 dissolved in 5% EtOH, green, and to 5% EtOH only, blue). Scale bar = 10 μm **(D)** Single DA1-PN (red) and the 14 KCs (green) postsynaptic to the DA1-PN bouton indicated by the arrow. Tracings performed on the EM FAFB dataset (Zheng et al., 2018). Square brackets indicate location of MBC. Different green shades represent different KC subtypes (as in E). Numbers in brackets in the legend represent the number of cells. **(E)** Single EM section through the MG (arrow in D). Scale bar = 1 μm. White square is magnified in left top panel with arrow pointing to a T-bar of the AZ and * labelling fine dendritic postsynaptic profiles of KCs. **(F)** Single plane confocal image of the MBC displaying PN boutons (blue; *α*-synapsin antibodies); the PSDs of KCs (green; *MB247-Dα7::GFP*) and the AZs of DA1-PN boutons only (red; *R37H08-Gal4 > UAS-brp-short*^{cherry}) identifying the cVA-responsive MGs. Scale bar = 10 μm. The MG in the white square is magnified in the right panels. **(G)** Automated

3D reconstruction of a confocal stack, including the image shown in (F). The reconstruction of MGs is based on Dα7-GFP (green) (see also Figure S1) and MGs receiving presynaptic input from DA1-PNs are marked by Brp–short^{cherry} (red). All other MGs are in green. Full genotypes used and statistics for all Figures are included in the Supplementary Table 2.

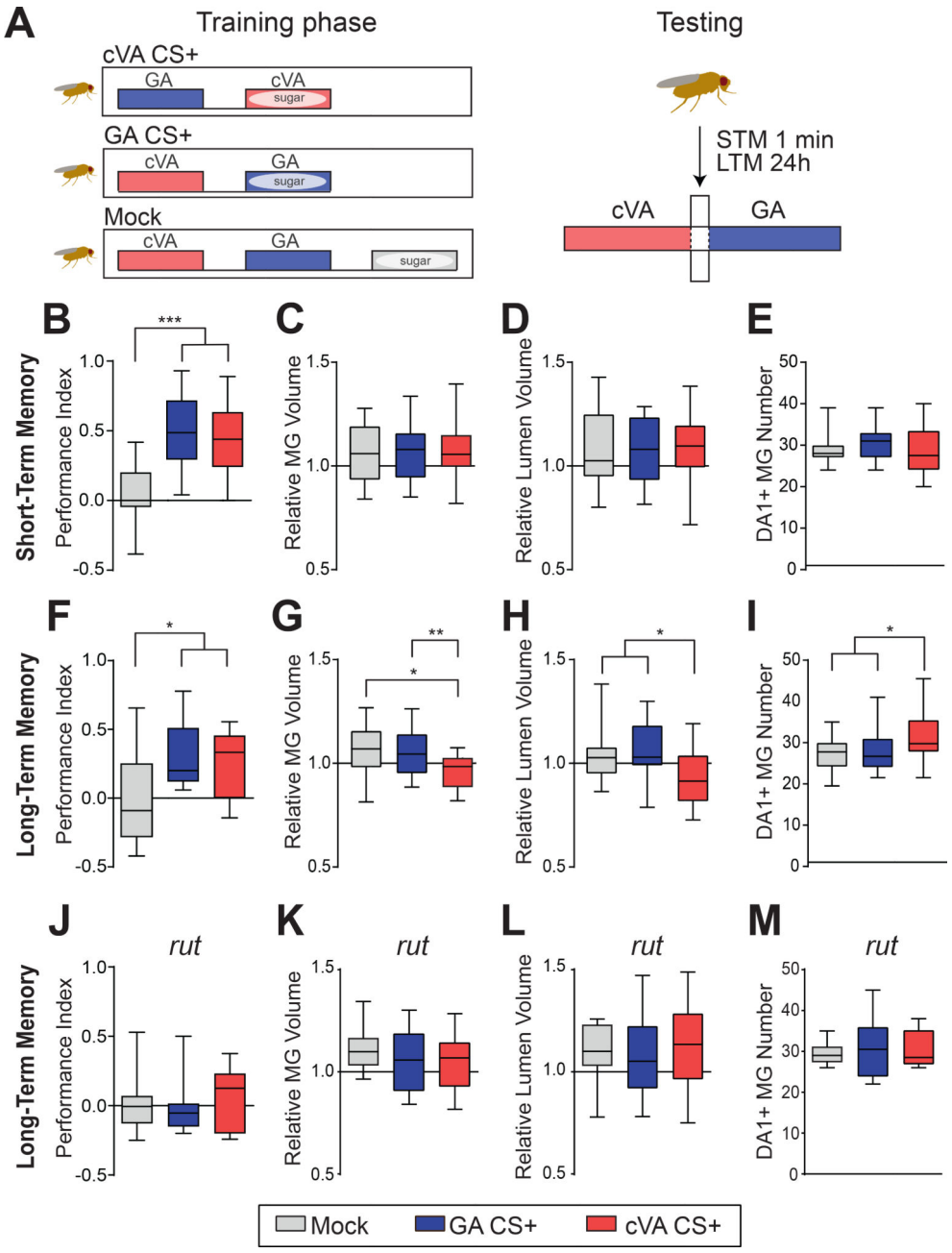

Figure 2 |. Microglomeruli undergo structural changes upon appetitive long-term memory formation

(A) Schematic illustration of the appetitive conditioning paradigm. For training, the conditioned odor cVA (red box) or GA (blue box) is paired with sugar. In STM experiments flies are trained for 2 min with a 2 min interval between CS+ and CS− presentation and tested 1 min after training. In LTM experiments flies are trained for 5 min + 5 min with a 2 min stimulus interval and are tested 24 h after training. In the mock control the two odors and the sugar reward are presented in a temporally spaced sequence with a 2 min inter-stimulus pause. **(B, F, J)** Performance indices of flies *R37H08-Gal4/MB247-DαGFP, UAS-brp-short*^{cherry} in the STM (**B,** ***$p < 0.001$, $n = 19–25$), or in the LTM paradigm

(**F**, *p < 0.05, n = 14–19) and performance index of *rut* mutant flies in LTM (**J**, $p > 0.05$, n = 17–18). Performance index values of the mock control group (grey) were compared to groups trained with GA CS+ (blue) or cVA CS+ (red). Multiple comparisons are tested throughout this study with one-way ANOVA with Bonferroni correction. Significance level is set at $p < 0.05$. *p < 0.05, ****p < 0.0001. **(C, G, K)** The MG volume comprises the volume contained within a ring of *MB247-Da7::GFP* PSDs and the volume of the *MB247-Da7::GFP* PSDs. **(D, H, L)** The MG lumen is the volume contained within a ring of *MB247-Da7::GFP* PSDs (see Figure S1D). In STM the relative volume (ratio of the average DA1-MG / non-DA1-MG per animal) of DA1- MGs **(C)** and of their lumen **(D)** is not different between groups ($p > 0.05$, n = 15–20). In LTM the relative MG volume **(G)** and lumen volume **(H)** of DA1- MGs in flies trained with cVA CS+ are smaller than in flies from the mock control group or of flies trained with GA CS+ (*p < 0.05, **p < 0.01, n = 19–25). **(E, I, M)** Number of DA1-PN positive MGs is unaffected in STM (**E,** $p > 0.05$, n = 18–24). In LTM, number of DA1-PN positive MGs in cVA CS+ trained flies is higher compared to flies of the mock control or GA CS+ group (**I, ***p < 0.05, n = 18–24). The structural modifications of DA1- MGs in cVA CS+ trained flies after the appetitive LTM protocol were suppressed in *rut* mutants (**K-M,** $p > 0.05$, n = 13–21). In all box plots, the edges of the boxes are the first and third quartiles, thick lines mark the medians, and whiskers represent data range.

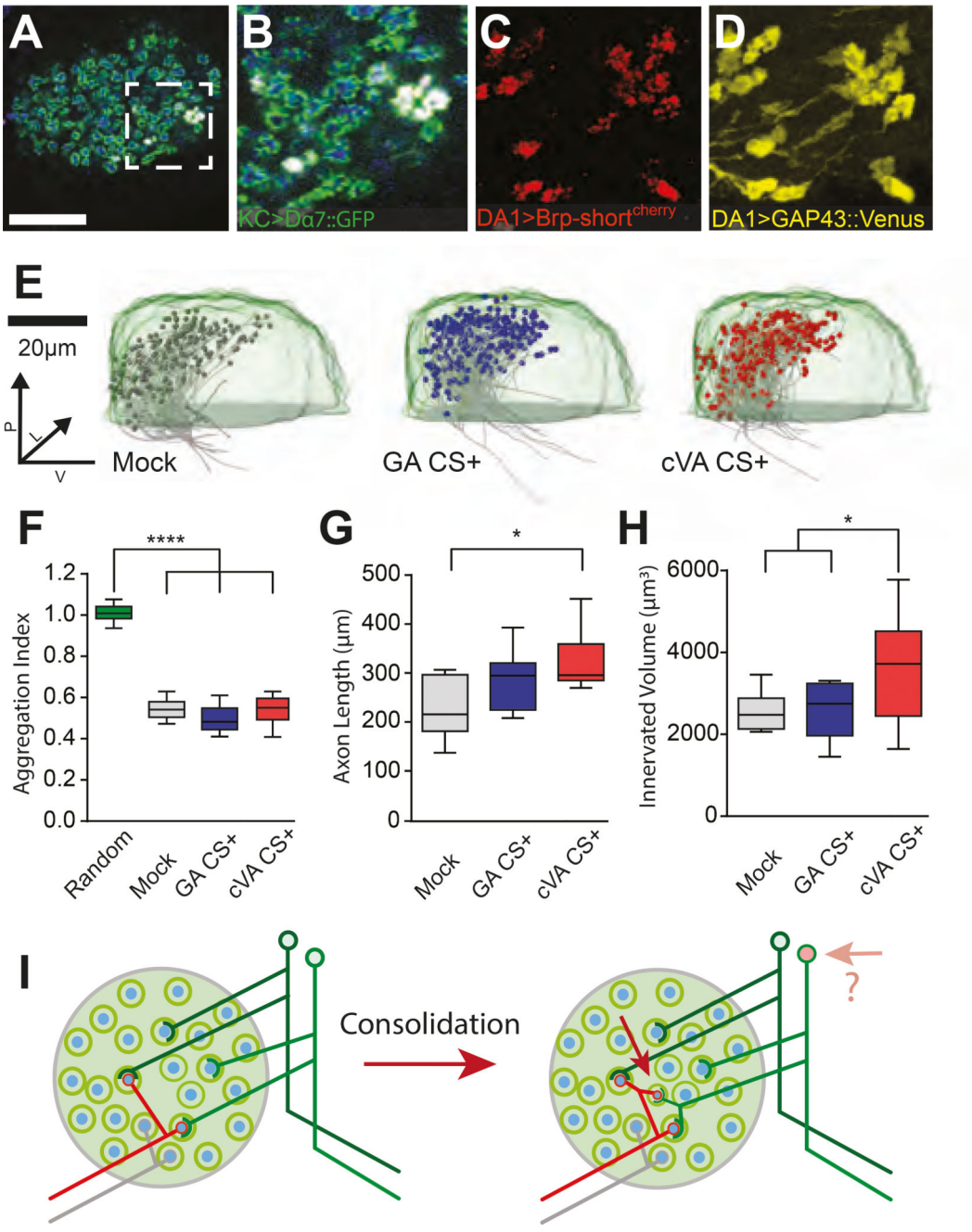

Figure 3 |. Modifications of axon collaterals and wiring properties of projection neurons within the mushroom body calyx after long-term memory formation

(A) Single optical section of the MBC of flies expressing Dα7GFP (green) in the KCs and Brp-short^{cherry} (red) plus GAP43-Venus (yellow) in DA1-PNs (*R37H08-Gal4*); PN boutons (blue; anti-Synapsin antibodies). Scale bar = 20 µm. **(B-D)** Magnification of the white square in (A) displaying the merge as in A **(B)** or a maximum-intensity projection of Brp-short^{cherry} **(C)** or of GAP43-Venus **(D)** signals. **(E)** Medial view of registered PN axons (grey) with traced boutons (grey, blue, red spheres) within a standard calyx (light green). The registered PN traces are of mock (grey), GA CS+ (blue) or cVA CS+ (red)

trained groups. n = 10 for each group. **(F)** Boutons are highly clustered independently of the treatment (Clark and Evans Aggregation index compared to a hypothetical random distribution. ****p < 0.0001, n = 10). **(G)** Total collateral axons length of mock control, GA CS+ or cVA CS+ flies. (*p < 0.05, n = 10). **(H)** The convex hull volume containing all DA1-boutons in the MBC per condition is increased in cVA CS+ flies compared to mock control and GA CS+ group (*p < 0.05, n = 10). **(I)** We suggest that the increased number of MGs after consolidation is due to the formation of additional boutons responding to cVA. The additional boutons form full MGs, as postsynaptic profiles of KCs surround them. It is unclear whether this reorganization might lead to the recruitment of additional responding KCs (see Discussion). In all box plots, the edges of the boxes are the first and third quartiles, thick lines mark the medians, and whiskers represent data range.

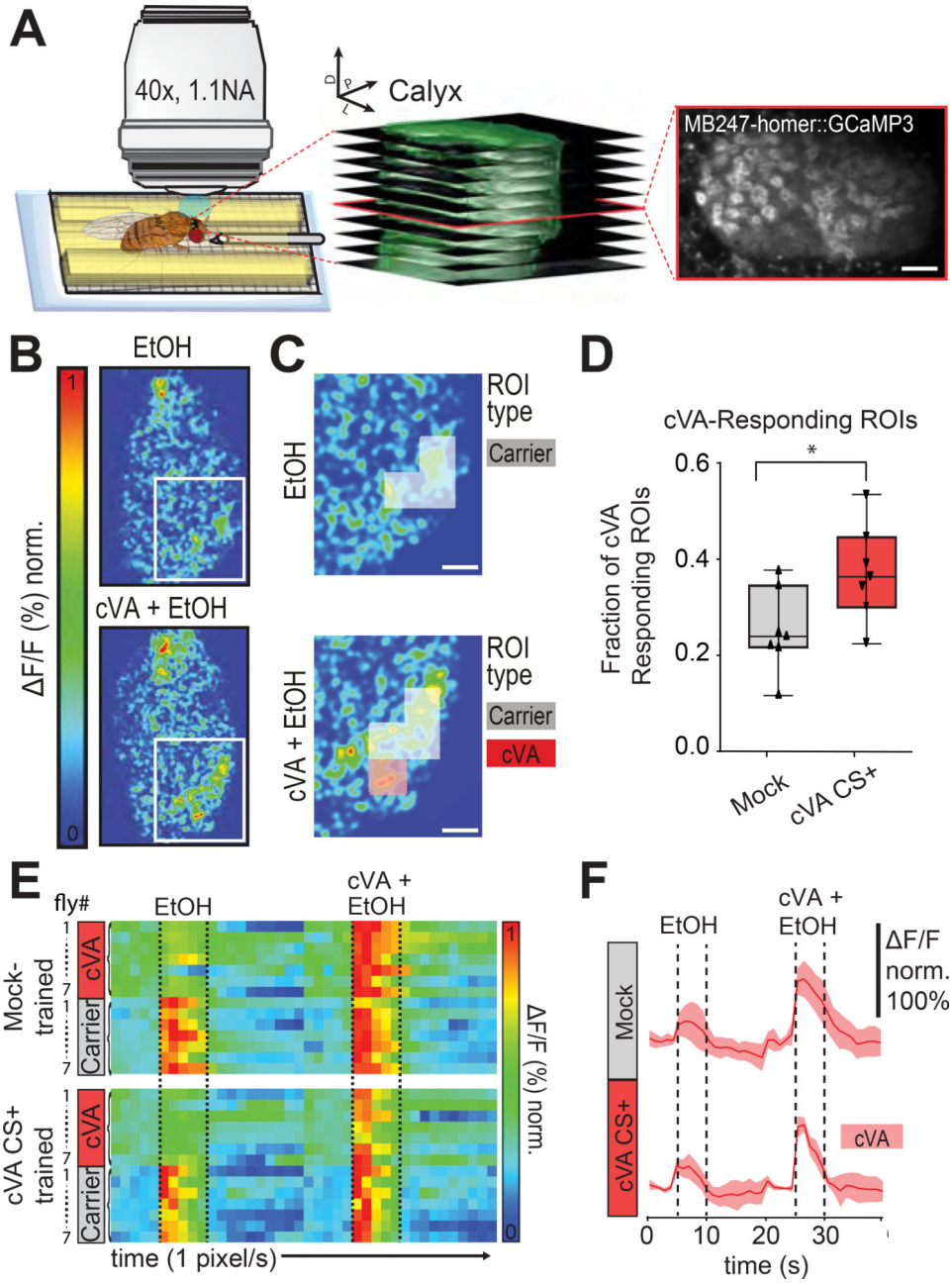

Figure 4 |. Functional plasticity in the mushroom body calyx associated with long-term memory

(A) Two-photon *in vivo* imaging setup. Schematic of a fly placed on a custom-made holder under a two-photon microscope equipped with a 40× 1.1 NA water immersion objective. The odor is delivered for 5s with a moisturized, constant air stream through a 1.2mm cannula. (Central panel) Z series of the entire MBC volume of flies expressing post-synapse-tagged Homer-GCaMP3 imaged during odor application at 1Hz (10 optical sections per volume, 4μm step size). (Right panel) A single slice of the image stack shown in the middle panel. Scale bar = 10 μm. **(B)** Representative optical section from a volumetric time series showing false-coloured response of KC dendrites to 5 s exposure to EtOH (top) or cVA + EtOH (bottom). **(C)** Magnification of the white square area in (B). 5×5 μm2 ROIs were

classified as cVA-responsive (red) if they were only active during cVA + EtOH application, but did not respond to EtOH alone. ROIs that responded to both conditions were classified as Carrier. Scale bar = 5 μm. **(D)** The fraction of cVA responsive ROIs increased after LTM acquisition compared to the mock control (box plot represent first and third quartiles, thick lines mark the medians, and whiskers represent data range. *$p < 0.05$, $n = 7$). **(E)** Dynamics of ΔF/F% changes over time in KCs of *MB247-homer::GCaMP3* flies after mock training (top) or LTM acquisition (bottom). Each row of the heat map represents average responses per animal of all cVA responsive ROIs (red) or of all carrier EtOH responsive ROIs (grey) within one MBC over time. Each column represents one 1s. Flies are first exposed to the EtOH (5s) and then to cVA + EtOH (5s) as indicated by the dashed lines. **(F)** Plot of average calcium dynamics over time of cVA responsive ROIs during 5 s stimulation with EtOH or with cVA in EtOH (dashed lines) in mock-trained (top) or cVA CS+ (bottom) flies ($n = 7$). Data represented as mean ± std.